Applied Thermal Engineering 31 (2011) 1613–1620

Contents lists available at ScienceDirect

Applied Thermal Engineering

journal homepage: www.elsevier.com/locate/apthermeng

Comparative study of different desiccant wheel designs

R. Narayanan [a,*], W.Y. Saman [a,1], S.D. White [b], M. Goldsworthy [b]

[a] Sustainable Energy Centre, University of South Australia, J2/02, Mawson Lakes Campus, Mawson Lakes, Adelaide, SA 5095, Australia
[b] CSIRO Energy Centre, 10 Murray Dwyer Circuit, Steel River Estate, Mayfield West, NSW 2304, Australia

ARTICLE INFO

Article history:
Received 27 August 2010
Accepted 25 January 2011
Available online 12 March 2011

Keywords:
Desiccant wheel
Solid-side resistance
Gas-side resistance
Dehumidification
Regeneration

ABSTRACT

Desiccant/evaporative cooling systems offer an environmentally benign alternative to conventional vapor compression chillers. A desiccant wheel is the heart of this heat driven cooling system and it uses a solid desiccant for dehumidification with silica gel being the most widely used. Proper design of the wheel is important for the successful operation of the system and theoretical models are useful tools in predicting the performance and optimizing the design. In this paper, two heat and mass transfer models of a counter flow desiccant wheel, one considering only the gas-side resistance, and the other considering both solid-side and gas-side resistances are developed. The models show good agreement with experimental data. The model is used to conduct a comparative study on the performance of different wheel designs. The study shows that the introduction of an axial cooling section can improve the performance of the wheel considerably.

1. Introduction

Evaporative cooling systems offer an inexpensive and environmentally friendly option for cooling of buildings, but they are not effective for high humidity climates. Desiccant/evaporative cooling systems are suitable for wider ranges of climates. They operate on an open heat-driven cycle consisting of a combination of a dehumidifier, a sensible heat exchanger and evaporative coolers. In this environmentally friendly system, dehumidification of air to low humidity level is done using a desiccant wheel so that evaporative cooling or other cooling options can be employed effectively to reduce the temperature of air.

A desiccant wheel is the heart of the heat driven cooling system and it uses a solid desiccant for dehumidification. The desiccant material is coated, impregnated or formed in place on the supporting rotor structure. The matrix consists of multiple channels in the direction of the axis of the wheel rotation. The wheel constantly rotates through two separate air streams, the supply air which is dried by the desiccant and hot regeneration air which reactivates the desiccant. The regeneration and supply air sides are separated by clapboard. The flow passage of the desiccant wheel is usually of sinusoidal shape and so this paper focuses on a desiccant wheel with sinusoidal channels.

As shown in Fig. 1, the components of a desiccant dehumidifying cassette include a desiccant wheel with a matrix consisting of supporting material and desiccant material, clapboard, wheel case, driving motor, hot regeneration air stream as well as the supply air to be dehumidified.

2. Heat and mass transfer in desiccant wheel

The transport phenomena occurring in a desiccant wheel have been investigated by many researchers over the years. The adsorption of water vapor from air involves many physical processes which offer resistances to vapor transfer from the gas phase to solid phase. These resistances of heat and mass transfer in this hygroscopic matrix can be categorized into two groups namely gas-side and the solid-side resistances. The gas-side resistance is the resistance of vapor transport from bulk gas to the surface of the solid desiccant, whereas the solid-side resistance is the resistance for transport of the adsorbed molecules into the pore structure of the desiccant material from the surface of the desiccant [1]. The gas-side resistance is mainly due to convective heat and mass transfer between the air and the desiccant. Solid-side resistance is due to heat conduction and mass diffusion within the desiccant. The vapor can diffuse through pores of the desiccant by three different ways, namely, ordinary diffusion, Knudsen diffusion and surface diffusion. All these mass transfer mechanisms can be predicted using Fickian type expressions with different diffusion coefficients, D_o, D_k and D_s. These coefficients can be estimated by the following expressions [2].

* Corresponding author. Fax: +61 8 830 23380.
E-mail address: ramadas.narayanan@unisa.edu.au (R. Narayanan).
[1] Fax: +61 8 830 23380.

1359-4311/$ – see front matter © 2011 Elsevier Ltd. All rights reserved.
doi:10.1016/j.applthermaleng.2011.01.043

Nomenclature

a	channel height (m)
A_d	surface area (m^2)
b	channel width (m)
c	channel length (m)
cp_d	specific heat capacity of desiccant (J/kg K)
cp_g	specific heat capacity of air (J/kg K)
D_a	combined ordinary and Knudsen diffusivity (m^2/s)
D_h	hydraulic diameter of the channel (m)
D_k	Knudsen diffusivity (m^2/s)
D_o	ordinary diffusivity (m^2/s)
D_s	surface diffusivity (m^2/s)
Le	Lewis number (−)
M_1	molecular weight of water (kg/kmol)
Nu	Nusselt number (−)
P_a	atmospheric pressure (Pa)
P_{in}	perimeter of flow channel (m)
q_a	heat of adsorption (J/kg)
T_d	temperature of air inside the control volume 2 (K)
T_g	temperature of air inside the control volume 1 (K)
u_g	velocity of supply air and regeneration air (m/s)
W_d	water vapor content of desiccant (kg/kg)
Y_g	humidity ratio of air inside the control volume 1 (kg/kg)
Y_d	humidity ratio of air inside the control volume 2 (kg/kg)
α	heat transfer coefficient (W/m^2 K)
β	mass transfer coefficient (kg/m^2 K)
ρ_g	density of air (kg/m^3)
ρ_d	density of desiccant (kg/m^3)
λ_d	thermal conductivity of the desiccant (W/m K)
φ	relative humidity of air (−)

$$D_o = 1.758 \times 10^{-4} \frac{T_d^{1.685}}{P_a} \quad (1)$$

$$D_s = \frac{1}{\zeta} D_o \exp\left(-0.9740 \times 10^{-3} \frac{q_a}{T_d} \right) \quad (2)$$

$$D_k = 97a \left(\frac{T_d}{M_1} \right)^{1/2} \quad (3)$$

With T_d being the temperature of desiccant (K), P_a the atmospheric pressure and ζ the tortuosity of the path of the pore, a is the pore radius and M_1 is the molecular weight of water, q_a is the heat of adsorption.

A large number of mathematical models have been developed to predict the heat and mass transfer behavior in air dehumidification applications with rotary desiccant wheels and a comprehensive literature review of all these models are done by Ge et al. [12]. By studying the literature of existing models of desiccant wheels, the existing theoretical models of desiccant wheels can be broadly classified into two categories based on the inclusion of various resistances considered for building the model. They are gas-side resistance model and gas and solid-side resistance model. The gas-side resistance model considers the heat and mass transfer resistances only in the bulk gas and solid-side resistances are ignored [3–6]. Among the gas and solid-side resistance models, most of them consider heat conduction and mass diffusion in one dimension only [1,7–8,10] whereas a few consider in two dimensions [2,9,11]. Some investigators consider all the three diffusions in the solid-side [2], but a few take Knudsen and surfaces diffusions [9] and some consider only surface diffusion [10].

Many of the existing studies focus on optimizing operational parameters like rotation speed, regeneration temperature, but none focus on different wheel design variations like variation in the direction of flow, comparison performance of existing and new designs. So this study focuses on these design variations.

3. Governing equations

The desiccant wheel can be considered as set of identical axial channels coated with desiccant. Fig. 2 shows a representative channel with the air control volume and desiccant control volume for the derivation of the governing equations. Even though the heat and mass transfer within the wheel will be in all three dimensions, simplifications are needed to enable the analysis [3–5]. Consequently, the following assumptions are made. In order to investigate the significance of the two resistances categorized under gas-side and solid-side resistances, two different models namely gas-side resistance (GSR) model and gas and solid-side resistance (GSSR) model are developed.

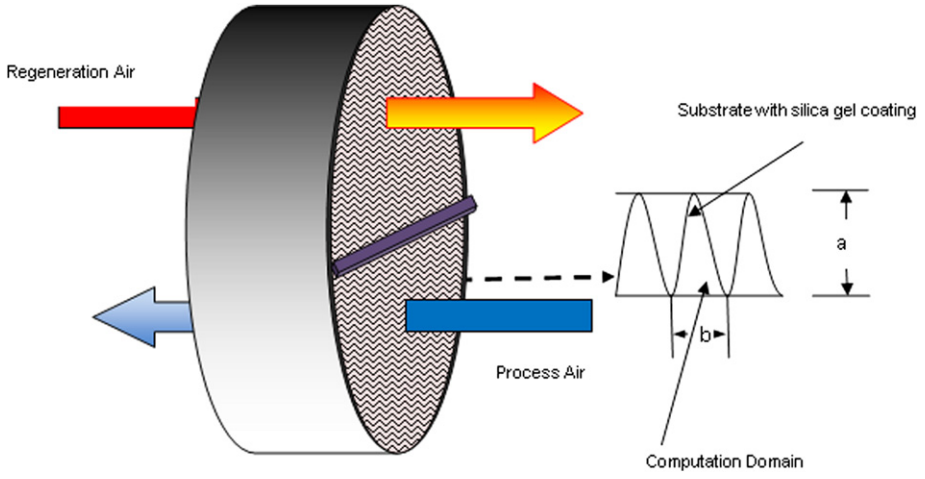

Fig. 1. Desiccant wheel.

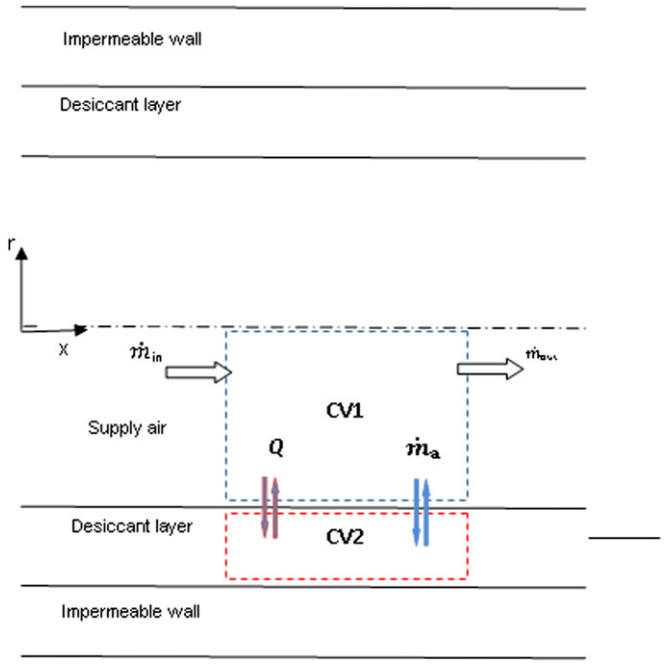

Fig. 2. Control volumes for the modelling.

3.1. Gas and solid-side resistance model

1. The desiccant wheel is a cylindrical wheel of length L and radius r with identical sinusoidal flow channels with its walls coated with the adsorbent silica gel. For simplicity it is divided into two equal sections: the dehumidification section and the regeneration section.
2. It is assumed that the movement of the wheel is so slow that the rate of mass and energy variation due to air flow in the circumferential direction can be neglected.
3. Heat conduction and mass diffusion in the gas-side are negligible and only convective heat and mass transfer takes place in the gas.
4. There are no radial or circumferential temperature or moisture content gradients in the matrix.
5. Hysteresis in the sorption isotherm for the desiccant coating is neglected and the heat of sorption is assumed as constant.
6. The matrix's thermodynamic properties and the mass and heat transfer coefficients are constant.
7. The air flow approaching each section will be turbulent, but within the channel, the flow will be laminar as the hydraulic diameter of channel is small, generally less than 5 mm and the values of velocity of approaching air will be low, generally less than 3 m/s. Therefore, air flow is assumed to be purely axial in direction and laminar. It is also assumed that the mass flow rate and velocity are constant for both the supply and regeneration streams.
8. Lewis number for the flow is assumed to equal to 1, so values of thermal and mass diffusivities are equal.

With these assumptions the mass and energy balance equations for the air and desiccant control volumes can be derived.

Mass balance in CV1

$$\frac{1}{u_g}*\frac{\partial Y_g}{\partial t}+\frac{\partial Y_g}{\partial x}=\frac{4\beta}{u_g D_h}(Y_d-Y_g) \tag{4}$$

Energy balance in CV1

$$\frac{1}{u_g}*\frac{\partial T_g}{\partial t}+\frac{\partial T_g}{\partial x}=\frac{4\alpha}{u_g D_h c_{pg}}(T_d-T_g) \tag{5}$$

Mass balance in CV2

$$\rho_g\frac{\partial Y_d}{\partial t}+\rho_d\frac{\partial W_d}{\partial t}=\rho_g D_a\frac{\partial^2 Y_d}{\partial t^2}+\rho_d D_s\frac{\partial^2 W_d}{\partial t^2}+\frac{\beta\rho_g P_{in}}{A_d}(Y_g-Y_d) \tag{6}$$

Energy balance in CV2

$$\rho_d c_t\frac{\partial T_d}{\partial t}=\lambda_d\frac{\partial^2 T_d}{\partial x^2}+\frac{\alpha P_{in}}{A_d}(T_g-T_d)+q_a\rho_d\frac{\partial W_d}{\partial t} \tag{7}$$

Equations (4)–(7) will be the governing equations for GSSR model.

3.2. Gas-side resistance model

For a gas-side resistance model, the solid-side resistances are neglected. So the mass and energy balance equations (4) and (5) for in CV1 remains same, but the diffusive and conductive terms of equations (6) and (7) will not be there. Therefore, the second and third terms in the right hand side of equation (6) and first term in the right hand side of equation (7) will disappear and the new equations will be as given below.

Mass balance in CV2

$$\rho_g\frac{\partial Y_d}{\partial t}+\rho_d\frac{\partial W_d}{\partial t}=\frac{\beta\rho_g P_{in}}{A_d}(Y_g-Y_d) \tag{8}$$

Energy balance in CV2

$$\rho_d c_t\frac{\partial T_d}{\partial t}=\frac{\alpha P_{in}}{A_d}(T_g-T_d)+q_a\rho_d\frac{\partial W_d}{\partial t} \tag{9}$$

So equations (4), (5), (8) and (9) will form the governing equations of the GSR model.

4. Auxiliary equations

The governing equations have five unknown variables Y_g, Y_d, W_d, T_g and T_d. To solve these simultaneous equations, one of the variables has to be eliminated. This can be done by relating the equilibrium humidity ratio of air Y_d to the water content, W_d and

Table 1
Model parameters and constants.

$Y_{g\,in}$	Inlet humidity ratio of supply air (kg/kg)	0.0142
$T_{g\,in}$	Inlet temperature of supply air (°C)	35
$Y_{g\,in1}$	Inlet humidity ratio of regeneration air (kg/kg)	0.0182
$T_{g\,in1}$	Inlet temperature of regeneration air (°C)	120
t_p, t_r	Time period for dehumidification and regeneration process (s)	90
c_{pl}	Isobaric specific heat capacity of water (liquid) (J/kg/K)	4181.3
c_{pv}	Isobaric specific heat capacity of water vapor (J/kg/K)	1872
k_a	Thermal conductivity of air (W/m K)	0.0263
ρ_g	Density of air (kg/m^3)	1.204
ρ_d	Density of desiccant (kg/m^3)	720
f_d	Mass fraction of the desiccant in the wheel	0.7
a	Channel height (m)	1.75×10^{-3}
b	Channel width (m)	3.5×10^{-3}
L	Channel length (m)	0.2
d	Desiccant layer thickness (m)	0.15×10^{-3}
c_{pd}	Isobaric specific heat capacity of desiccant (J/kg/K)	921
c_{pg}	Isobaric specific heat capacity of air (J/kg/K)	1009
u_g	Velocity of supply air and regeneration air (m/s)	2
SR	Supply regeneration area ratio (−)	0.5

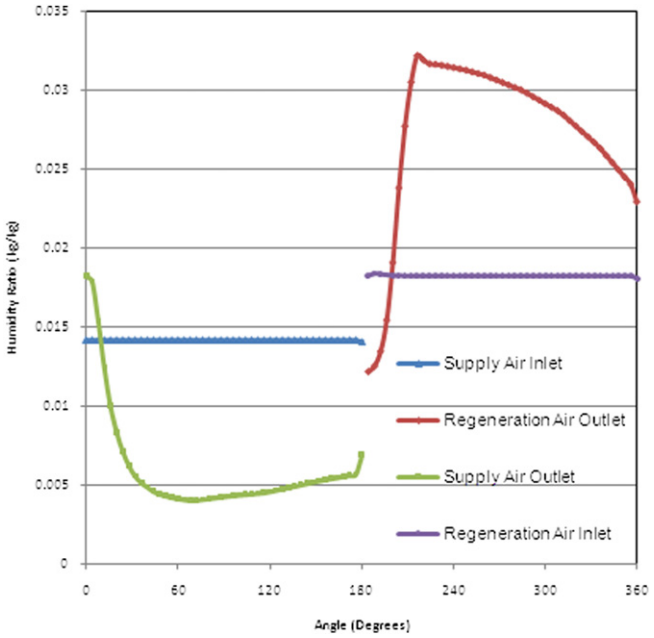

Fig. 3. Inlet and outlet humidity ratio profiles.

temperature of the desiccant, T_d. So an equilibrium isotherm relationship of silica gel can be used.

The equilibrium humidity content of regular density silica gel is governed by the following isotherm relationship [1].

$$\varphi = 0.0078 - 0.05759W_d + 24.16554W_d^2 - 124.78W_d^3 + 204.226W_d^4 \quad (10)$$

where W_d is the water content and φ is the relative humidity of air.

The heat of adsorption is determined by using the following expression [1].

$$q_a = \begin{cases} -12,400W_d + 3500 & W_d \le 0.05 \\ -1400W_d + 2900 & W_d > 0.05 \end{cases} \quad (11)$$

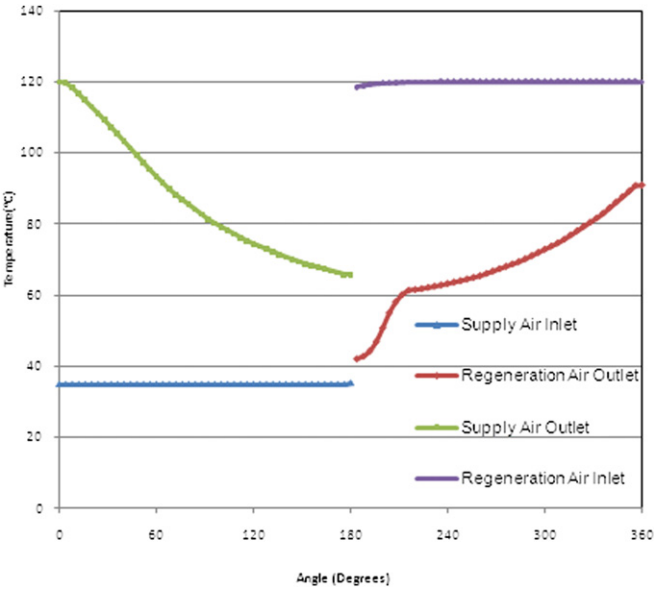

Fig. 4. Inlet and outlet temperature profiles.

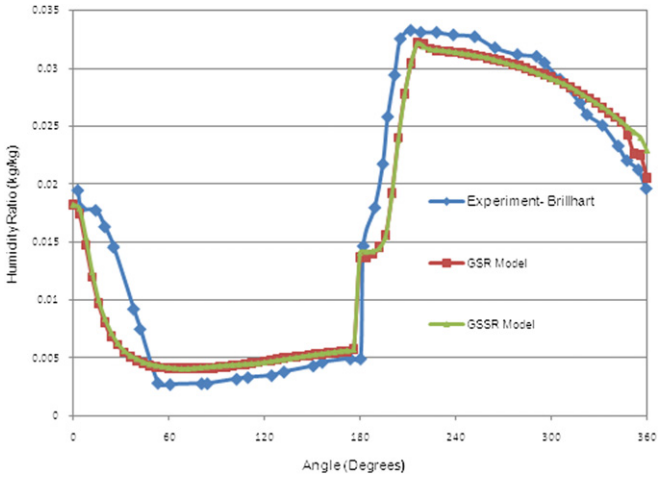

Fig. 5. Humidity ratio profile.

Using psychrometric relations, the relative humidity and humidity ratio are given below [2].

$$\frac{\varphi}{Y_d} + 1.61\varphi = 10^{-6}e^{5294/T_d} \quad (12)$$

Since the channel geometry is assumed to be sinusoidal, the following expression can be used to calculate the hydraulic diameter [7].

$$D_h = a\left[1.0542 - 0.466^*\left(\frac{a}{b}\right) - 0.1180^*\left(\frac{a}{b}\right)^2 + 0.1794\left(\frac{a}{b}\right)^3 - 0.043\left(\frac{a}{b}\right)^4\right] \quad (13)$$

The convective heat and mass transfer coefficients can be calculated from Nusselt number and Lewis number respectively. For the sinusoidal shaped channel, these coefficients can be calculated using the following expressions.

$$Nu_T = 1.1791\left(1 + 2.0771\left(\frac{a}{b}\right) - 3.1901\left(\frac{a}{b}\right)^2 - 1.9975\left(\frac{a}{b}\right)^3 - 0.4966\left(\frac{a}{b}\right)^4\right) \quad (14)$$

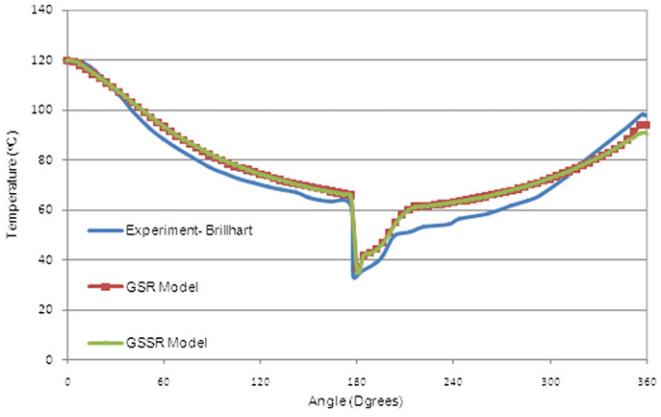

Fig. 6. Outlet temperature profile.

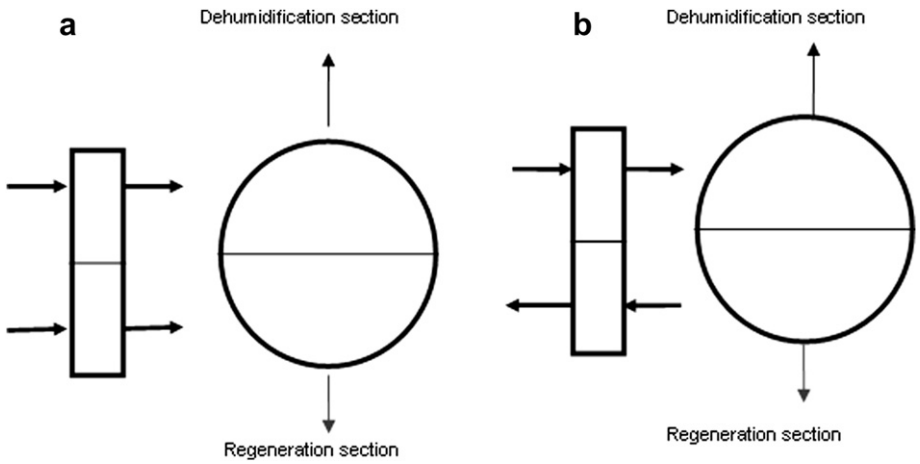

Fig. 7. a. Parallel flow design. b. Counter flow design.

$$\mathrm{Nu_H} = 1.903\left(1 + 0.455\left(\frac{a}{b}\right) + 1.2111\left(\frac{a}{b}\right)^2 - 1.6805\left(\frac{a}{b}\right)^3 + 0.7724\left(\frac{a}{b}\right)^4 - 0.1228\left(\frac{a}{b}\right)^5\right) \quad (15)$$

$$\mathrm{Nu} = (\mathrm{Nu_T} + \mathrm{Nu_H})/2 \quad (16)$$

$$\mathrm{Nu} = \frac{\alpha}{\lambda_a D_h} \quad (17)$$

$$\mathrm{Le} = \frac{\alpha}{\rho_g \beta c_{pg}} \quad (18)$$

4.1. Boundary and initial conditions

The above governing equations are subjected to the following initial and boundary conditions.

For the supply air section,

$Y_g(t,0) = Y_{g\ in}$
$T_g(t,0) = T_{g\ in}$
$T_d(0,x) = T_d(t_r, L-x)$
$W_d(0,x) = W_d(t_r, L-x)$

For the regeneration section,

$Y_g(t,0) = Y_{g\ in1}$
$T_g(t,0) = T_{g\ in1}$
$T_d(0,x) = T_d(t_p, L-x)$
$W_d(0,x) = W_d(t_p, L-x)$

The wall boundaries are assumed to be adiabatic and impermeable.

5. Results

The governing equations for the gas-side resistance model and the gas and solid-side resistance model are solved using COMSOL Multiphysics which is finite element analysis, solver and simulation software for coupled partial differential equations. The input data are used for the simulation are given in Table 1. Since the supply air and regeneration sections assumed to be equal, angles for both sections will be 180° and the ratio between the area of supply air section and regeneration air (SR ratio) is 0.5.

Figs. 3 and 4 show the outlet humidity ratio and temperature profiles obtained from the model for a counter flow desiccant wheel. During the dehumidification process, the outlet humidity ratio decreases sharply at the beginning and reaches a minimum value and then increases gradually until the end of the dehumidification

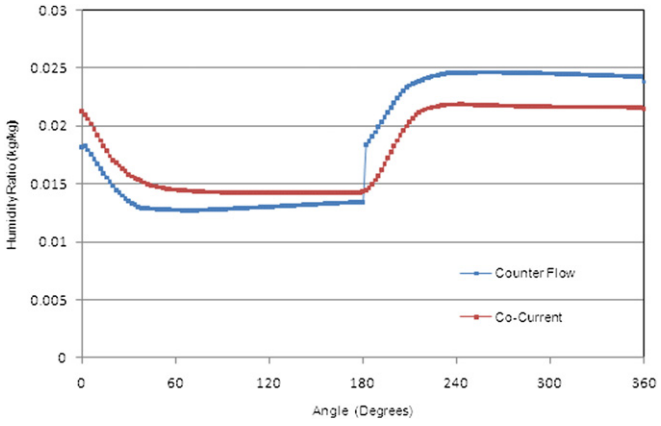

Fig. 8. HR profile of the two designs.

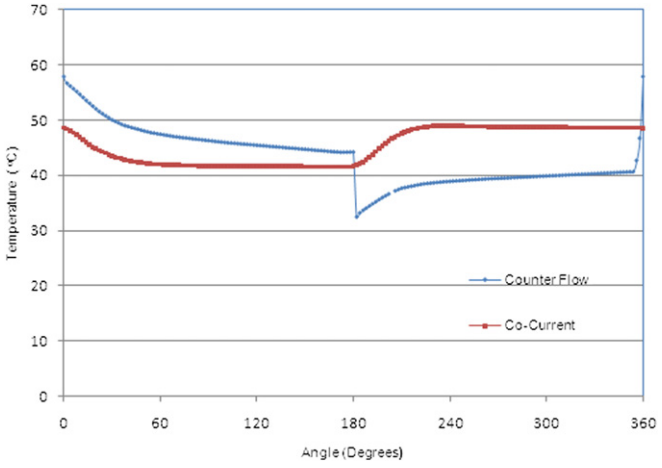

Fig. 9. Temperature profile of the two designs.

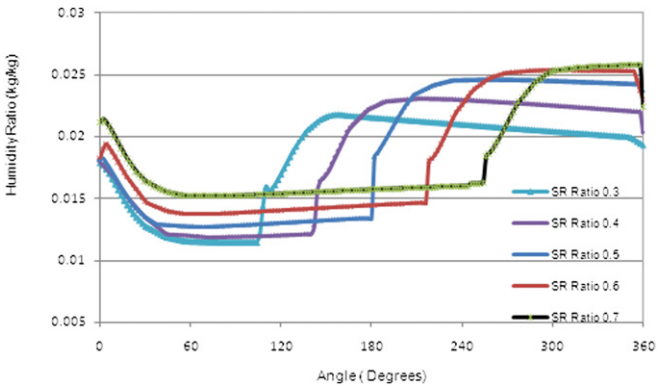

Fig. 10. HR profile for wheels with various SR ratio.

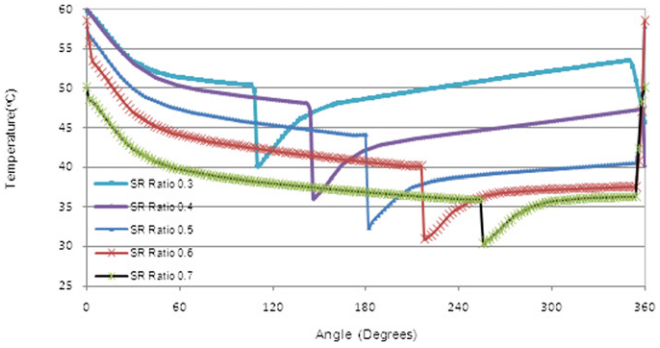

Fig. 11. Temperature profile for wheels with various SR ratio.

process whereas for regeneration, the humidity ratio of air rises sharply at the beginning and then gradually declines. The sharp edge in the start of regeneration air outlet humidity curve is due to effects of the sudden transition from dehumidification to regeneration section where air is coming in opposite direction. Temperature of air at the outlet drops from the regeneration temperature steadily during dehumidification. Throughout the regeneration process, the temperature increases, but slightly at a faster rate the beginning.

6. Experimental validation

In Figs. 5 and 6, the outlet humidity ratio and temperature results of the model are compared with the experimental results of Brillhart [13]. It can be observed that model has good agreement with experimental outlet humidity ratio and temperature. As in the case of previous works [4,11], the deviation of the humidity ratio curve from the experimental value may be attributed greater experimental uncertainties at the beginning of dehumidification period. The figures also demonstrate that at the selected operating condition, the effect of solid-side resistance is negligible.

7. Effect of varying design parameters

The impact of varying the design parameters is investigated by analyzing the performance of the various designs. The parameters varied are the direction of flow of the regeneration air stream, supply/regeneration section area ratio and introduction of additional axial cooling stream. For the comparison the inlet conditions are chosen according to the summer design temperature data for Brisbane, Australia, i.e. 29.7 °C dry bulb temperature and 24.9 °C wet bulb temperature [14].

7.1. Flow direction

For a parallel flow desiccant wheel, the direction of the supply and regeneration air streams is the same whereas for a counter flow desiccant wheel, these directions will be opposite as shown in Fig. 7a and b.

In order to incorporate these variations in the direction of flow streams, the boundary conditions and the values of velocity of air are to be implemented as given below.

For counter flow arrangement, during the dehumidification period,

$$Y_g(t,0) = Y_{g\ in}$$
$$T_g(t,0) = T_{g\ in}$$
$$u_g = 2\ \text{m/s}$$

For the regeneration period,

$$Y_g(t,L) = Y_{g\ in1}$$
$$T_g(t,L) = T_{g\ in1}$$
$$u_g = -2\ \text{m/s}$$

For parallel flow arrangement, during the dehumidification period,

$$Y_g(t,0) = Y_{g\ in}$$
$$T_g(t,0) = T_{g\ in}$$
$$u_g = 2\ \text{m/s}$$

For the regeneration period,

$$Y_g(t,0) = Y_{g\ in1}$$
$$T_g(t,0) = T_{g\ in1}$$
$$u_g = 2\ \text{m/s}$$

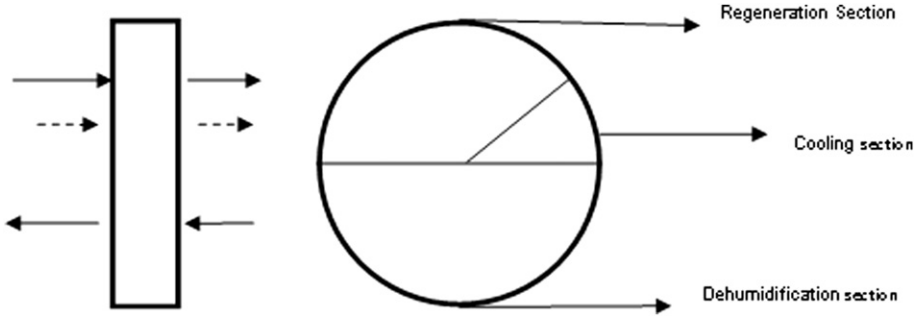

Fig. 12. Counter flow desiccant wheel with an axial cooling section.

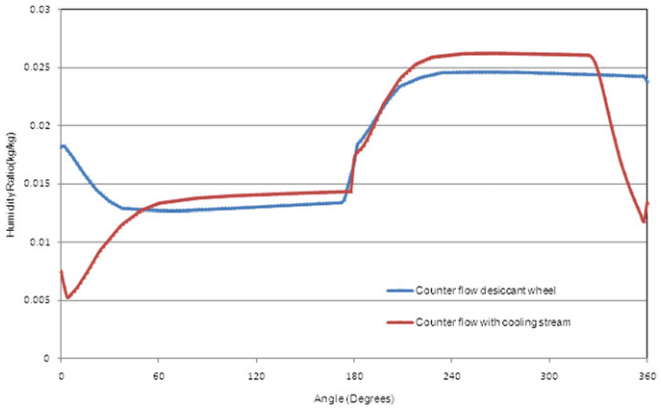

Fig. 13. HR profile of two designs.

Figs. 8 and 9 show the humidity ratio and temperature of air at outlet of parallel flow and counter flow configurations. As expected, it is evident that the counter flow arrangement has better dehumidification performance, but the temperature at the outlet of the supply air is much higher than that of parallel flow configuration.

7.2. Supply/regeneration section area ratio

The ratio between the supply air section area and regeneration air section area not only determines the quantity of supply air that can be handled by the wheel but also influences the dehumidification and regeneration performance. As the value of this ratio increases, the dehumidification section area increases and regeneration area decreases. Keeping the supply air and regeneration air velocities constant, enlarging the dehumidification section will result in the ability of the wheel to handle a higher rate of supply air, but may result in partial regeneration of the desiccant. If this ratio is small, this will result in a reduction in the quantity of supply air, a complete removal of water vapor during the regeneration and better dehumidification performance. A smaller dehumidification section also contributes to the increased effect of the carry-over heat from the regeneration process. This is evident in Figs. 10 and 11 which show the humidity and temperature results for supply/regeneration area ratios of 0.3, 0.4, 0.5, 0.6 and 0.7. In this case, it is evident that larger the regeneration area, lower will be the humidity ratio of air at outlet of dehumidification section. This can be attributed to more effective regeneration due to larger regeneration area.

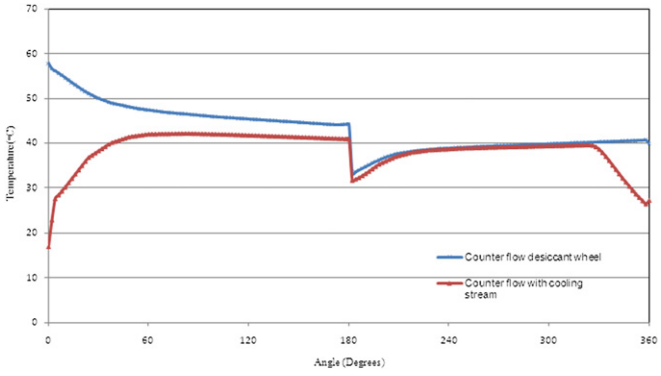

Fig. 14. Temperature profile of two designs.

Table 2
Comparison of performance of 3 designs (supply air inlet humidity ratio is 0.018 kg/kg and temperature is 29.7 °C).

Type	Average outlet humidity ratio (kg/kg)	Average outlet temperature (°C)	% Dehumidification	Change in sp. enthalpy (kJ/kg)
Parallel flow	0.01507	42.56	16.27	5.517
Counter flow	0.01350	47.32	25.05%	6.447
Counter flow with axial cooling section	0.01264	39.81	29.77%	−3.583

7.3. Introduction of an additional cooling stream

The regeneration process not only removes the water vapor from the desiccant matrix, but also increases the temperature of the matrix which reduces the dehumidification capacity of the desiccant material. If the temperature of the desiccant is brought down before the dehumidification can bring in greater deduction in the humidity ratio of the supply air. So in the new design, an additional cooling air stream is introduced after the regeneration process. For producing this air, air at outlet of evaporative cooler will be the ideal choice. Fig. 12 shows the counter flow desiccant wheel with an axial cooling stream.

This modification is incorporated in the model by specifying additional boundary condition for the cooling period as given below.

$$Y_g(t,0) = Y_{gc}$$
$$T_g(t,0) = T_{gc}$$
$$u_g = 2 \text{ m/s}$$

Figs. 13 and 14 compare the outlet humidity and temperature for conventional counter flow desiccant wheel and a counter flow desiccant wheel with an axial cooling stream. The conventional desiccant wheel has SR ratio of 0.5. The one with axial cooling stream has 180° for the dehumidification section whereas the regeneration section has 144° and the cooling section occupies 36°. With this arrangement, the temperature and humidity ratio of cooling stream air is 15 °C and 0.008 kg/kg respectively. The velocities of flow for all streams are assumed as 2 m/s. Energy balance of the model is carried out and the percentage error is found as less than 1%.

It is evident from the graph that introduction of axial cooling stream can improve the dehumidification performance considerably at initial part and also bring the outlet temperature to much lower level. This arrangement provides an air stream at conditions closer to comfort provision.

8. Summary and conclusions

The comparison of the outlet conditions for the three designs is shown in Table 2. Here the percentage dehumidification is calculated as the percentage of reduction in humidity relative to the inlet humidity ratio.

Heat and mass transfer models considering gas-side and solid-side resistance are developed for counter flow desiccant wheel and the results show good agreement with experimental data. A comparison of performance of different designs of wheel is conducted. Results shows that at the selected design conditions, the percentage dehumidification rate of parallel flow, simple counter flow and counter flow with cooling section are 16.27% 25.05% and 29.77% respectively. Therefore, counter flow desiccant wheel has

much better dehumidification performance than parallel flow, whereas the addition of axial cooling section can improve both dehumidification and cooling performance further.

Acknowledgements

This project is funded by University of South Australia and Commonwealth Scientific and Industrial Research Organization, Australia.

References

[1] A. Pesaran, Moisture Transport in Silica Gel Particle Beds, Ph.D. Thesis, University of California, Los Angeles, 1983.
[2] L.Z. Zhang, J.L. Niu, Performance comparisons of desiccant wheels for air dehumidification and enthalpy recovery, Applied Thermal Engineering 22 (2002) 1347–1367.
[3] X.J. Zhang, Y.J. Dai, R.Z. Zhang, A simulation study of heat and mass transfer in a honeycombed rotary desiccant dehumidifier, Applied Thermal Engineering 23 (8) (2003) 989–1003.
[4] J.D. Chung, D.Y. Lee, S.M. Yoon, Optimization of desiccant wheel speed and area ratio of regeneration to dehumidification as a function of regeneration temperature, Solar Energy 83 (5) (2009) 625–635.
[5] K. Tsutsui, S. Yamaguchi, K. Saito, N. Onda, Effect of design and operating conditions on performance of desiccant wheels, in: IRR HVAC Energy Efficiency Best Practice Conference, Melbourne, 2008.
[6] R. Narayanan, W.Y. Saman, S.D. White, M. Goldsworthy, IIR Gustav Lorentzen Conference, Sydney, April 2010.
[7] C.R. Ruivo, J.J. Costa, A.R. Figueiredo, Analysis of simplifying assumptions for NM of HMT in a porous medium, Numerical Heat Transfer: Part A 49 (2006) 851–872.
[8] C.R. Ruivo, J.J. Costa, A.R. Figueiredo, Numerical study of the cyclic behaviour of a desiccant layer of hygroscopic rotor, Numerical Heat Transfer 48 (2008) 1037–1053.
[9] C.R. Ruivo, J.J. Costa, A.R. Figueiredo, On the behavior of hygroscopic wheels: part 1: channel modeling, International Journal of Heat and Mass Transfer 50 (2007) 4812–4822.
[10] Z. Gao, V.C. Mei, J.J. Tomlinson, Theoretical analysis of dehumidification process in a desiccant wheel, Heat and Mass Transfer 41 (2005) 1033–1042.
[11] L.A. Sphaier, L.M. Worek, Analysis of heat and mass transfer in porous sorbents used in rotary regenerators, International Journal of Heat and Mass Transfer 47 (2004) 3415–3430.
[12] T.S. Ge, Y. Li, R.Z. Wang, Y.J. Dai, A review of the mathematical models for predicting rotary desiccant wheel, Renewable and Sustainable Energy Reviews 12 (2008) 1485–1528.
[13] P.L. Brillhart, Evaluation of Desiccant Rotor Matrices Using an Advanced Fixed-Bed Test System, Ph.D. Thesis, University of Illinois, Chicago, 1997.
[14] AIRAH Technical Handbook. Australian Institute of Refrigeration and Air-conditioning and Heating, Melbourne, 2007.